Scaling analysis and simulation of strongly stratified turbulent flows

G. BRETHOUWER[1], P. BILLANT[2], E. LINDBORG[1] AND J.-M. CHOMAZ[2]

[1]Linné Flow Centre, KTH Mechanics, KTH, SE-100 44 Stockholm, Sweden
geert@mech.kth.se

[2]LadHyX, Ecole Polytechnique, F-91128 Palaiseau Cedex, France

Direct numerical simulations of stably and strongly stratified turbulent flows with Reynolds number $Re \gg 1$ and horizontal Froude number $F_h \ll 1$ are presented. The results are interpreted on the basis of a scaling analysis of the governing equations. The analysis suggests that there are two different strongly stratified regimes according to the parameter $\mathscr{R} = Re F_h^2$. When $\mathscr{R} \gg 1$, viscous forces are unimportant and l_v scales as $l_v \sim U/N$ (U is a characteristic horizontal velocity and N is the Brunt–Väisälä frequency) so that the dynamics of the flow is inherently three-dimensional but strongly anisotropic. When $\mathscr{R} \ll 1$, vertical viscous shearing is important so that $l_v \sim l_h/Re^{1/2}$ (l_h is a characteristic horizontal length scale). The parameter $\mathscr{R}$ is further shown to be related to the buoyancy Reynolds number and proportional to $(l_O/\eta)^{4/3}$, where l_O is the Ozmidov length scale and η the Kolmogorov length scale. This implies that there are simultaneously two distinct ranges in strongly stratified turbulence when $\mathscr{R} \gg 1$: the scales larger than l_O are strongly influenced by the stratification while those between l_O and η are weakly affected by stratification. The direct numerical simulations with forced large-scale horizontal two-dimensional motions and uniform stratification cover a wide Re and F_h range and support the main parameter controlling strongly stratified turbulence being $\mathscr{R}$. The numerical results are in good agreement with the scaling laws for the vertical length scale. Thin horizontal layers are observed independently of the value of $\mathscr{R}$ but they tend to be smooth for $\mathscr{R} < 1$, while for $\mathscr{R} > 1$ small-scale three-dimensional turbulent disturbances are increasingly superimposed. The dissipation of kinetic energy is mostly due to vertical shearing for $\mathscr{R} < 1$ but tends to isotropy as $\mathscr{R}$ increases above unity. When $\mathscr{R} < 1$, the horizontal and vertical energy spectra are very steep while, when $\mathscr{R} > 1$, the horizontal spectra of kinetic and potential energy exhibit an approximate $k_h^{-5/3}$-power-law range and a clear forward energy cascade is observed.

1. Introduction

Stable and strong stratification is a common phenomenon in the atmosphere, oceans and lakes. Owing to their importance for the understanding of geophysical flows, stratified flows have been investigated in many theoretical, experimental and numerical studies. A commonly observed feature of strongly and stably stratified flows in the laboratory and numerical simulations is the formation of quasi-horizontal layers, often described as pancake structures (Herring & Métais 1989; Waite & Bartello 2004; Praud, Fincham & Sommeria 2005; Basak & Sarkar 2006 among others).

This typical feature is also predicted by theoretical turbulence models (Godeferd & Cambon 1994). Billant & Chomaz (2000a) investigated the dynamics of vertical columnar vortices in a strongly stratified fluid and observed the development of a zigzag instability ultimately leading to the formation of decoupled pancake-like vortices with sharp vertical gradients. They conjectured that the zigzag instability is the generation mechanism for the layered structures found in laboratory-scale flows and in geophysical flows. A main issue is the stability and the dynamics of these pancake-like structures in stratified turbulent flows: do they break-up into smaller structures and so cause a forward cascade of energy, or do the structures merge and hence cause an inverse cascade?

Mesoscale spectra of the kinetic and potential energy in the atmosphere display regularly a $k_h^{-5/3}$ and a k_v^{-3} power-law behaviour, where k_h and k_v are the horizontal and vertical wavenumber respectively (Nastrom & Gage 1985; Cot 2001). Several hypotheses have been developed to explain the observed spectra in stable stratified geophysical flows. Gage (1979) and Lilly (1983) attributed the $k_h^{-5/3}$ spectrum to an inverse cascade of energy as in two-dimensional turbulence. Herring & Métais (1989) performed numerical simulations of strongly stratified turbulence and reported only a weak inverse cascade. Métais *et al.* (1996) have also performed simulations of stratified and rotating flows and could only observe the inverse cascade in the strongly rotating limit when $N/f \sim 1$, but not in the strongly stratified limit with $N/f \gg 1$, which is relevant to the mesoscale range. Dewan (1979, 1997), on the other hand, suggested the existence of a forward cascade generated by gravity waves. To explain the $k_h^{-5/3}$-spectrum, Lindborg (2002, 2006) proposed the hypothesis of strongly anisotropic three-dimensional turbulence in stratified flows, associated with a forward cascade of energy. Numerical simulations employing an *ad hoc* subgrid-scale model subsequently confirmed this hypothesis: the horizontal $k_h^{-5/3}$ spectrum was reproduced and a forward cascade of energy was clearly observed. Such a forward energy cascade with inertial characteristics and horizontal $k_h^{-5/3}$ spectrum was, however, not found in some other previous numerical simulations and laboratory experiments.

Smith & Waleffe (2002) carried out numerical simulations of stratified flows with forcing at relatively small scales and argued for an energy transfer from small to large scales whenever the Froude number F_h is smaller than a critical value. They observed a very slow monotonic growth of the kinetic energy in the simulations and all energy piled-up in the $k_h = 0$ mode (often called the shear mode) when the stratification was strong. Such a growth of the energy in the shear mode was not always observed in simulations of strongly stratified flows by Laval, McWilliams & Dubrulle (2003). At low Re (Reynolds number) the fluid appeared to be stable, but when Re was increased in steps at a fixed F_h (horizontal Froude number), they saw more frequently regions with small or negative Ri (Richardson number) signifying the existence of shear instabilities and overturning of the buoyancy field. The slope of the horizontal energy spectrum was, nevertheless, much steeper than $k_h^{-5/3}$. Laval *et al.* suggested that shear instabilities will occur, whatever the strength of the stratification, if Re is large enough.

Randomly forced flows with varying F_h were studied numerically by Waite & Bartello (2004). When the stratification was weak, the flow resembled three-dimensional isotropic turbulence but the flow became increasingly layered when the stratification was increased. At low F_h, the layers were very stable and no overturning motions were observed. The spectra at low F_h were similar to the spectra obtained from a reduced set of equations, based on the assumption of a small vertical Froude

number, but Waite & Bartello noted that they did not resemble the spectra in the atmosphere. The simulations showed increasing anisotropy of the dissipation tensor with increased stratification. In a following study, Waite & Bartello (2006) employed randomly forced internal gravity waves to generate turbulence. They investigated whether breaking waves could reproduce spectra observed in the atmosphere and oceans but concluded that the simulations were unsuccessful in this respect and furthermore noted that the spectra were sensitive to Re.

Riley & deBruynKops (2003) carried out direct numerical simulations (DNS) of decaying stratified flows initialized with perturbed Taylor–Green vortices. Growing horizontal shear layers were observed between the vortices when the flow developed, creating local regions with small Ri. This led to the development of Kelvin–Helmholtz-type rollers, which subsequently became unstable and broke down to three-dimensional turbulence. The horizontal spectra showed an approximate but limited $k_h^{-5/3}$-range, suggesting inertial-range dynamics. They argued that the large-scale motions in stratified flows can be a continuous source of energy for smaller-scale motions and generate turbulence, provided Re is large enough. In experiments by Praud *et al.* (2005) of decaying stratified turbulence, layers were observed and the vertical shearing was intense in the fluid, but it did not appear to be strong enough to produce overturning instabilities. Horizontal spectra did not reveal a $k_h^{-5/3}$ power law.

Kitamura & Matsuda (2006) studied spectra in stratified turbulence through large-scale simulations. With rotation the horizontal $k_h^{-5/3}$ spectrum was reproduced and a forward energy cascade was observed, but without rotation, the horizontal spectrum was steeper. They noted that the energy dissipation due to vertical shearing was significant, even at large scales, and this may have affected the results.

The cascade of energy from large to small scales in stably stratified flows has now been confirmed by many independent studies (Lindborg 2002, 2006; Riley & deBruynKops 2003; Waite & Bartello 2004, 2006; Kitamura & Matsuda 2006). Moreover, examinations of atmospheric data support the forward energy cascade hypothesis (Cho & Lindborg 2001; Lindborg & Cho 2001). The aforementioned studies also share the notion of horizontal layer formation and strong vertical shear, but the extracted spectra showed large variations. Furthermore, shear instabilities and overturning motions are observed in some studies but not all. These discrepancies in the results must necessarily be the consequence of the different conditions under which the studies are performed. Naturally, F_h is a key parameter and also Re has been shown to have a significant influence on turbulence in stratified flows, but the studies do not give a definite answer to how the flow features are related to Re and F_h. An additional problem faced in laboratory and numerical experiments is that it is impossible to reach the same combination of Re and F_h as in geophysical flows. Stratified flows studied in the laboratory or by simulations always reach small F_h at the expense of a relatively low Re and therefore they are perhaps not fully representative of the flows found outdoors.

The main objective of our study is to investigate the influence of Re and F_h on the dynamics of strongly stratified flows and in particular on turbulence, length scales, spectra and instabilities. Through DNS of stratified flows with an extensive Re and F_h range results of a scaling analysis of the governing equations are validated. This should contribute to a better understanding and a clearer interpretation of the dynamics of strongly stratified flows and a more precise design of future laboratory and numerical experiments so that these more closely resemble stratified geophysical flows.

2. Scaling analysis

2.1. *Governing equations*

The equations of motions of a stratified, incompressible flow under the Boussinesq approximation are

$$\frac{\partial \boldsymbol{u}'}{\partial t'} + \boldsymbol{u}' \cdot \nabla' \boldsymbol{u}' = -\frac{1}{\rho_0} \nabla' p' + \nu \nabla'^2 \boldsymbol{u}' - \frac{\rho' g}{\rho_0} \boldsymbol{e}_z, \tag{2.1}$$

$$\nabla' \cdot \boldsymbol{u}' = 0, \tag{2.2}$$

$$\frac{\partial \rho'}{\partial t'} + \boldsymbol{u}' \cdot \nabla' \rho' = \kappa \nabla'^2 \rho' - \frac{\partial \overline{\rho}}{\partial z'} u'_z, \tag{2.3}$$

where $\boldsymbol{u}'$ is the velocity, u'_z the vertical velocity component, p' the pressure, ν and κ the viscosity and diffusivity respectively, g the acceleration due to gravity, ρ_0 a constant reference density, $\boldsymbol{e}_z$ the unit vector in the vertical direction and ρ' a perturbation from the linear density profile $\overline{\rho}$. The Brunt–Väisälä frequency, defined as $N = \sqrt{-(g/\rho_0)\partial\overline{\rho}/\partial z'}$, is assumed constant.

2.2. *Scaling of the equations*

To understand the dynamics of stably stratified flows, the governing equations are analysed using scaling arguments, thereby briefly recapitulating the analysis of Billant & Chomaz (2001), Godoy-Diana, Chomaz & Billant (2004) and Lindborg (2006). This analysis will facilitate the interpretation of the results presented later in the paper and obtained in other studies.

For an arbitrary scale in the fluid with characteristic horizontal velocity and length scale U and l_h respectively, and vertical length scale l_v, we introduce the aspect ratio $\alpha = l_v/l_h$ and the horizontal Froude number $F_h = U/(l_h N)$. Following Riley, Metcalfe & Weismann (1981) and Billant & Chomaz (2001), the horizontal velocity is scaled by U, the vertical velocity by UF_h^2/α, the horizontal and vertical length by l_h and l_v respectively, the time by l_h/U, ρ' by $U^2\rho_0/(gl_v)$ and the pressure by $\rho_0 U^2$, leading to

$$\frac{\partial \boldsymbol{u}_h}{\partial t} + \boldsymbol{u}_h \cdot \nabla_h \boldsymbol{u}_h + \frac{F_h^2}{\alpha^2} u_z \frac{\partial \boldsymbol{u}_h}{\partial z} = -\nabla_h p + \frac{1}{Re}\left[\frac{1}{\alpha^2}\frac{\partial^2 \boldsymbol{u}_h}{\partial z^2} + \nabla_h^2 \boldsymbol{u}_h\right], \tag{2.4}$$

$$F_h^2\left[\frac{\partial u_z}{\partial t} + \boldsymbol{u}_h \cdot \nabla_h u_z + \frac{F_h^2}{\alpha^2} u_z \frac{\partial u_z}{\partial z}\right] = -\frac{\partial p}{\partial z} - \rho + \frac{F_h^2}{Re}\left[\frac{1}{\alpha^2}\frac{\partial^2 u_z}{\partial z^2} + \nabla_h^2 u_z\right], \tag{2.5}$$

$$\nabla_h \cdot \boldsymbol{u}_h + \frac{F_h^2}{\alpha^2}\frac{\partial u_z}{\partial z} = 0, \tag{2.6}$$

$$\frac{\partial \rho}{\partial t} + \boldsymbol{u}_h \cdot \nabla_h \rho + \frac{F_h^2}{\alpha^2} u_z \frac{\partial \rho}{\partial z} = u_z + \frac{1}{ReSc}\left[\frac{1}{\alpha^2}\frac{\partial^2 \rho}{\partial z^2} + \nabla_h^2 \rho\right], \tag{2.7}$$

where non-dimensional variables are denoted without a prime. Here $Re = Ul_h/\nu$, $Sc = \nu/\kappa$ is the Schmidt number, $\boldsymbol{u}_h$ and u_z are the horizontal and vertical velocity respectively, and ∇_h is the horizontal gradient. In the limit of strong stratification, i.e. $F_h = U/(l_h N) \to 0$, and $Re \gg 1$, we obtain from (2.4)–(2.7)

$$\frac{\partial \boldsymbol{u}_h}{\partial t} + \boldsymbol{u}_h \cdot \nabla_h \boldsymbol{u}_h + \frac{F_h^2}{\alpha^2} u_z \frac{\partial \boldsymbol{u}_h}{\partial z} = -\nabla_h p + \frac{1}{Re\,\alpha^2}\frac{\partial^2 \boldsymbol{u}_h}{\partial z^2}, \tag{2.8}$$

$$0 = -\frac{\partial p}{\partial z} - \rho, \tag{2.9}$$

$$\nabla_h \cdot \boldsymbol{u}_h + \frac{F_h^2}{\alpha^2}\frac{\partial u_z}{\partial z} = 0, \tag{2.10}$$

$$\frac{\partial \rho}{\partial t} + \boldsymbol{u}_h \cdot \nabla_h \rho + \frac{F_h^2}{\alpha^2} u_z \frac{\partial \rho}{\partial z} = u_z + \frac{1}{ReSc\alpha^2} \frac{\partial^2 \rho}{\partial z^2}, \tag{2.11}$$

where we have kept $O(F_h^2/\alpha^2)$ and $O(Re\alpha^2)$ terms because the value of α is unknown so far.

An additional, quite commonly made assumption is $l_v \gg U/N$, i.e. $\alpha \gg F_h$, together with $\alpha \gg 1/\sqrt{Re}$. The advection terms involving vertical derivatives in (2.8) and (2.11) can be neglected under these assumptions and the continuity equation (2.10) reduces to $\nabla_h \cdot \boldsymbol{u}_h = 0$ (Riley *et al.* 1981; Riley & Lelong 2000). The governing equation for $\boldsymbol{u}_h$ is then purely horizontal and this assumption therefore leads to the hypothesis that, although variations in the vertical direction are allowed and layers can develop, the dynamics of strongly stratified turbulence is similar to two-dimensional turbulence with an inverse cascade of energy (Lilly 1983; Lilly *et al.* 1998). The essential assumption behind this derivation is that l_v is not a free parameter but instead imposed by external factors in such a way that the vertical Froude number $F_v = U/(l_v N) \ll 1$.

In contrast to this, we adopt the point of view of Billant & Chomaz and Godoy-Diana *et al.* that l_v is a free parameter determined by the dynamics of the flow itself. Assuming $F_h \ll 1$ and $Re \gg 1$ and considering (2.8), we can distinguish two dynamically different regimes depending on the relative magnitude of the the vertical advection term, which is $O(F_h^2/\alpha^2)$, and the diffusion terms, which are $O(Re\alpha^2)$. The state of the flow is thus determined by the parameter $\mathscr{R} = ReF_h^2$ characterizing the ratio of the vertical advection and diffusion terms.

2.3. $\mathscr{R} = ReF_h^2 \gg 1$: the strongly stratified turbulence regime

If $\mathscr{R} \gg 1$, the viscous and diffusive terms in (2.8) and (2.11) can be neglected compared to $O(F_h^2/\alpha^2)$ terms (provided that $Sc \gtrsim 1$). The governing equations are then self-similar with respect to $z'N/U$, where z' is the vertical dimensional coordinate, as shown by Billant & Chomaz (2001). This suggests the scaling $l_v \sim U/N$, implying $\alpha \sim F_h$ and $F_v \sim 1$. The consequence of the scaling $l_v \sim U/N$ is that the vertical advection terms contribute to the leading dynamics which for this reason are three-dimensional but strongly anisotropic. Another consequence of this scaling is that the potential energy is of the same order as the kinetic energy (Billant & Chomaz 2001).

The scaling $l_v \sim U/N$ has been supported by simulations of stratified homogeneous turbulence (Godeferd & Staquet 2003; Waite & Bartello 2004) and it was revealed through linear stability analysis of vortex pairs in stratified flows (Billant & Chomaz 2000b). Also the experiments by Park, Whitehead & Gnanadeskain (1994) and Holford & Linden (1999) are consistent with this scaling.

Lindborg (2006) adopted the scaling $l_v \sim U/N$ and assumed it to be valid at all scales in the strongly stratified inertial range of turbulence. This led to the hypothesis, which we also adopt here, of a special type of three-dimensional turbulence in strongly stratified flows with a highly anisotropic forward energy cascade. We will call this the strongly stratified regime, sometimes abbreviated to 'stratified turbulence'. The perhaps most important underlying assumption of the forward-cascade hypothesis is that the horizontal length scale of the turbulent structures can be estimated as $l_h \sim U^3/\varepsilon$, where ε is the kinetic energy dissipation, similar to the integral length of isotropic turbulence (Taylor 1935). This estimate can be validated by assuming that there is a balance between advection and dissipation terms in the kinetic energy equation which can be derived from (2.8). We will use Taylor's estimate as the definition of the horizontal length scale and validate this *á posteriori* by comparing this length scale with the horizontal forcing length scale in our simulations. Applying

this definition, the Reynolds number, the Froude number and the parameter $\mathscr{R}$ can be rewritten as

$$Re = \frac{U^4}{\nu\varepsilon}, \qquad F_h = \frac{\varepsilon}{NU^2}, \qquad \mathscr{R} = \frac{\varepsilon}{\nu N^2}. \qquad (2.12)$$

Defined in this way the parameter $\mathscr{R}$ is also called the buoyancy Reynolds number (Smyth & Moum 2000). From the expression for F_h follows the length scale relations

$$\frac{l_h}{l_O} = F_h^{-3/2}, \qquad \frac{l_v}{l_O} \sim F_h^{-1/2}, \qquad (2.13)$$

where $l_O = \varepsilon^{1/2}/N^{3/2}$ is the Ozmidov length scale. Since it is required that $F_h \ll 1$, these relations show that the Ozmidov length scale sets a lower limit on the scales of stratified turbulence, in the horizontal as well as in the vertical. Lindborg (2006) made the estimate $F_h < 0.02$ for the limit under which stratified turbulence can be observed.

An interesting observation is that the parameter $\mathscr{R}$, as given by (2.12), does not include any length or velocity scale. According to the scaling analysis in the preceding section, $\mathscr{R}$ is the ratio between inertial and viscous forces in stratified turbulence. If it is assumed that both the scaling analysis and the Taylor estimate $l_h \sim U^3/\varepsilon$ are valid for 'eddies' or flow structures of different size l_h and different characteristic horizontal velocity scale U, then the influence of the viscosity is equally important at all scales of stratified turbulence. This is in contrast to Kolmogorov turbulence where the influence of viscosity decreases with increasing scale. However, this property of stratified turbulence does not rule out the possibility of an inertial range, because the influence will be very small at all scales when $\mathscr{R} \gg 1$.

The condition $\mathscr{R} \gg 1$ can also be written as

$$\mathscr{R} = \left(\frac{l_O}{\eta}\right)^{4/3} \gg 1, \qquad (2.14)$$

where $\eta = \nu^{3/4}/\varepsilon^{1/4}$ is the Kolmogorov scale. Since the Ozmidov length scale marks the transition between stratified and Kolmogorov turbulence the condition (2.14) implies that stratified turbulence can only exist in the presence of Kolmogorov turbulence at small scales. The Kolmogorov scale is to be resolved in a DNS. To simulate stratified turbulence we thus have to resolve not only all scales down to the Ozmidov length scale, but also a considerable range of smaller scales. Faced by these extraordinary computational demands it is natural to ask if the condition (2.14) can be relaxed in any way. If Navier–Stokes viscosity is replaced by hyperviscosity the condition (2.14) can indeed be relaxed (see Appendix A), but as long as Navier–Stokes viscosity is employed it must be fulfilled. To validate (2.14) further, we make an estimate of the energy dissipation in the large scales of stratified turbulence. With $l_v \sim U/N$, we obtain

$$\varepsilon_{Large} \sim \nu \frac{\partial u}{\partial z}\frac{\partial u}{\partial z}\bigg|_{Large} \sim \nu N^2 = \frac{\varepsilon}{\mathscr{R}}. \qquad (2.15)$$

With $\mathscr{R} \ll 1$, the large-scale dissipation would be larger than the total dissipation and we are faced with a contradiction, and thus $\mathscr{R} \ll 1$ is not consistent with $l_v \sim U/N$. If $\mathscr{R} \sim 1$, the large-scale dissipation would constitute a considerable fraction of the total dissipation. Only if $\mathscr{R} \gg 1$ is the large-scale dissipation negligible and an inertial range possible.

Using the instability criterion

$$Ri = \frac{-(g/\rho_0)(\partial\rho/\partial z)}{(\partial u_h/\partial z)^2} \simeq \frac{N^2}{(\partial u_h/\partial z)^2} \lesssim 1 \qquad (2.16)$$

for the existence of shear instabilities and the estimate $\partial u_h/\partial z \sim \sqrt{\varepsilon/\nu}$, Riley & deBruynKops (2003) suggested the condition $Ri^{-1} \sim \mathscr{R} > 1$ for the existence of Kolmogorov-like turbulence. This condition is thus similar to the one derived above, but the condition $\mathscr{R} \gg 1$ is more stringent. We would like to emphasize that whereas the condition of Riley & deBruynKops is concerned with the existence of local shear instabilities at small scales, our condition is concerned with the existence of an inertial cascade at scales larger than l_O. The Miles–Howard instability criterion can also be calculated for these large scales $l_h > l_O$. Using the estimate $\partial u_h/\partial z \sim U/l_v$ and scaling $l_v \sim U/N$, which is valid for all vertical scales dominated by stratification, we find $Ri \sim 1$. Consequently, we can argue that, through the zigzag instability and spontaneous formation of layers (Billant & Chomaz 2000a), intense vertical shear is generated that makes the flow susceptible to shear instabilities.

Just as in the case of Kolmogorov turbulence, scaling arguments (Lindborg 2006) suggest that the horizontal kinetic and potential energy spectra of stratified turbulence should have the form

$$E_K(k_h) = C_1 \varepsilon^{2/3} k_h^{-5/3}, \qquad E_P(k_h) = C_2 \varepsilon_P k_h^{-5/3}/\varepsilon^{1/3}, \qquad (2.17)$$

for horizontal wavenumbers, k_h, such that $k_h l_h \gg 1$ and $k_h l_O \ll 1$. Here, ε and ε_P are the dissipation of kinetic and potential energy respectively and C_1 and C_2 are two constants corresponding to the Kolmogorov and the Obukhov–Corrsin constants of Kolmogorov turbulence. Scaling arguments (Billant & Chomaz 2001; Lindborg 2006) also suggest that the vertical energy spectra should have the form

$$E_K(k_v) \sim E_P(k_v) \sim N^2 k_v^{-3}, \qquad (2.18)$$

for vertical wavenumbers, k_v, such that $k_v l_v \gg 1$ and $k_v l_O \ll 1$. It should be noted that the range of vertical wavenumbers where (2.18) can be valid is much more narrow than the range where (2.17) is supposed to be valid, which can be seen from the length-scale relations (2.13). With $F_h \sim 10^{-3}$, which is a reasonable value for geophysical flows, these relations suggest that the $k_h^{-5/3}$-range of the horizontal spectra should encompass three or four decades while the k_v^{-3}-range of the vertical spectra would not be broader than one decade. There are several other theories (e.g. Lumley 1964; Dewan & Good 1986; Hines 1991) that predict vertical energy spectra of the form (2.18) in different wavenumber ranges of geophysical flows. For a review of these theories see Waite & Bartello (2006).

2.4. $\mathscr{R} = ReF_h^2 \ll 1$: the viscosity-affected stratified flow regime

The case $\mathscr{R} \ll 1$ treated by Godoy-Diana *et al.* (2004) might be of less importance for geophysical flows where often $\mathscr{R} \gg 1$, but nonetheless it is relevant for numerical simulations and laboratory experiments of stratified flows. If $\mathscr{R} \ll 1$, the vertical advection term in (2.8) is negligible compared to the viscous term and the vertical interaction between layers and pancake vortices is predominantly through vertical viscous shearing. Assuming that the vertical length scale is a free parameter selected by the flow itself, Godoy-Diana *et al.* (2004) have argued that the vertical length scale can only be determined by a balance between the horizontal advection term and the vertical diffusion term. This is fulfilled if $Re\alpha^2 \sim 1$ (if we assume $Sc \gtrsim 1$ which is true

for most geophysical flows) giving

$$l_v \sim l_h Re^{-1/2}. \tag{2.19}$$

The vertical length scale is thus independent of the strength of the stratification and the non-dimensional governing equations (2.8)–(2.11) reduce to

$$\frac{\partial \boldsymbol{u}_h}{\partial t} + \boldsymbol{u}_h \cdot \nabla_h \boldsymbol{u}_h = -\nabla_h p + \frac{\partial^2 \boldsymbol{u}_h}{\partial z^2}, \tag{2.20}$$

$$0 = -\frac{\partial p}{\partial z} - \rho, \tag{2.21}$$

$$\nabla_h \cdot \boldsymbol{u}_h = 0, \tag{2.22}$$

$$\frac{\partial \rho}{\partial t} + \boldsymbol{u}_h \cdot \nabla_h \rho = u_z + \frac{1}{Sc} \frac{\partial^2 \rho}{\partial z^2}. \tag{2.23}$$

Riley & Lelong (2000), among others, derived a similar set of equations by directly assuming $F_v \ll 1$, but it was thought to describe stratified flows with strong viscous effects as well as without such effects. If $\mathscr{R} \ll 1$ the large-scale dynamics is determined by a balance between inertial and viscous forces due to vertical shearing. Therefore no inertial cascade can develop and the dissipation occurs predominantly at the largest scales. We call this regime the viscosity-affected stratified flow regime.

We can estimate the dissipation at large scales by $\varepsilon_{Large} = \nu \langle \partial u_h / \partial z \rangle^2 \sim \nu U^2 / l_v^2$. Assuming $\varepsilon_{Large} \simeq \varepsilon$ and using (2.19) we obtain $\varepsilon \sim U^3 / l_h$, i.e. Taylor's estimate is valid for viscosity-affected stratified flows as well. Relations (2.12) thus remain valid and we can estimate $Ri \simeq 1/\mathscr{R}$ showing that Kelvin–Helmholtz type of disturbances cannot be present when $\mathscr{R} \ll 1$. Praud *et al.* (2005) observed the scaling $\varepsilon \sim U^3 / l_h$ in their experiments where $Ri \gg 1$. The observed self-similarity in their experiments can thus be understood on basis of the present analysis for $\mathscr{R} \ll 1$, but, contrary to their claim, this situation does not resemble stratified flows at much higher Re because then $\mathscr{R} \gg 1$ and the dynamics described in §2.3 should take over.

3. Simulations

3.1. *Numerical methodology*

Homogeneous turbulence with a uniform and stable stratification is simulated to validate the hypotheses presented in §2. A standard pseudospectral method with periodic boundary conditions is employed to solve the Boussinesq equations (2.1), (2.2) and (2.3). The numerical domain is a rectangular box with sides L_h in the two horizontal directions and side L_v in the vertical. Time advancement of the equations is carried out with the classical fourth-order Runge–Kutta method for the nonlinear terms and exact integration of the viscous and diffusive terms. Aliasing errors arising from the computation of the nonlinear terms are suppressed by a combination of phase shifting and truncation.

Forcing is employed to simulate strongly stratified turbulent flows with high Reynolds numbers. An advantage of forcing is that the flow attains a statistically stationary state and this simplifies a parametric study of the influence of Re and F_h. Using an eddy-damped quasi-normal Markovian (EDQNM) closure model, Godeferd & Cambon (1994) showed that pure vortical interactions are dominant in strongly stratified turbulent flows and induce the strong anisotropy and layers. Forcing of the vortical modes therefore seems an efficient way to generate the desired anisotropic stratified turbulence. Like Herring & Métais (1989), Waite & Bartello

Run	Re ($\times 10^3$)	F_h ($\times 10^{-2}$)	$\mathscr{R}$	$\dfrac{L_h}{L_v}$	$N_h \times N_v$	$k_{max}\eta$	$\dfrac{l_h}{L_h}$	$\dfrac{l_v}{l_h}$	$\dfrac{\langle u_z^2 \rangle}{2E_K}$	$\dfrac{-\langle u_z'\rho \rangle}{u'_{z,rms}\rho'_{rms}}$
R0.3	1.2	1.5	0.29	2	80×48	1.1	1.0	0.064	0.004	0.17
R0.7	2.8	1.6	0.69	2.5	128×64	1.1	1.1	0.039	0.011	0.13
A0.06	11	0.23	0.058	4	256×64	1.1	1.6	0.020	0.0003	0.10
A0.2	7.3	0.53	0.21	4	256×64	1.1	1.2	0.025	0.0018	0.10
A0.8	5.0	1.2	0.75	4	256×64	1.1	0.9	0.030	0.008	0.11
A1.8	7.5	1.5	1.75	4	256×80	1.1	1.2	0.026	0.021	0.09
A2.8	5.5	2.3	2.84	4	256×64	1.1	1.0	0.040	0.038	0.11
A9.3	5.3	4.2	9.3	2.9	256×96	1.2	0.9	0.049	0.068	0.14
B0.1	21	0.23	0.11	6	512×96	1.1	1.3	0.014	0.0003	0.10
B0.4	20	0.45	0.40	6	512×96	1.1	1.3	0.014	0.0017	0.09
B1.1	17	0.81	1.09	6	512×96	1.1	1.1	0.017	0.009	0.07
B3.0	12	1.5	2.97	5	512×128	1.2	0.9	0.025	0.026	0.08
B9.3	13	2.7	9.3	4	512×144	1.2	0.9	0.032	0.049	0.09
C15.6	22	2.6	15.6	4	768×240	1.1	0.9	0.030	0.049	0.09
D0.1	50	0.16	0.13	9	960×128	1.0	1.2	0.009	0.0002	0.09
D0.5	31	0.39	0.47	9	960×128	1.1	0.9	0.011	0.0015	0.08
D1.6	28	0.75	1.57	9	960×128	1.1	0.8	0.014	0.008	0.06
D4.2	49	0.93	4.2	6	1024×192	1.1	1.3	0.016	0.020	0.06
D9.6	40	1.6	9.6	4	1024×320	1.1	1.1	0.019	0.028	0.06

TABLE 1. Overview of the numerical and physical parameters used in the simulations. N_h, N_v are the number of nodes in the horizontal and vertical direction respectively, l_v is computed as described in Appendix B and $\langle u_z'\rho' \rangle / u'_{z,rms}\rho'_{rms}$ is the mean buoyancy flux normalized by the r.m.s. of the vertical velocity fluctuations and density fluctuations. To distinguish series of simulations with (approximately) the same horizontal resolution and Re, the runs are labelled R, A, B, C and D. The additional number refers to the value of $\mathscr{R}$.

(2004) and Lindborg (2006) we opt for a purely horizontal forcing, implying that layer formation, vertical shear instabilities and the resulting vertical length scale are entirely the consequence of internal dynamics of the flow. In the DNS the forcing is restricted to horizontal vortical modes with $2\pi k_h/L_h \leqslant 3$ (the density field is not forced). The amount of forcing power injected at low wavenumbers is held constant by employing a method similar to the one proposed by Alvelius (1999). Lindborg (2006) used essentially the same forcing technique as we use, the only difference being the weak forcing of the vertical modes used by Lindborg which is omitted here. The simulations are initialized with random velocity fluctuations obeying a prescribed energy spectrum. This ensures that the large-scale, purely two-dimensional vortices induced by the forcing can become unstable through a mechanism such as the zigzag instability (Billant & Chomaz 2000a) leading to the spontaneous development of layers.

3.2. *Choice of the numerical and physical parameters*

Several DNS have been carried out within a quite wide range of values for Re and small F_h. The numerical and physical parameters used in the DNS are listed in table 1. The physical parameters are extracted from the DNS after the flow had reached statistical stationarity. The parameters have been chosen so that both regimes, $\mathscr{R} < 1$ and $\mathscr{R} > 1$, are covered by the simulations. The simulations are labelled R, A, B, C, D to distinguish the runs with (approximately) the same horizontal resolution. The additional number denotes the value of $\mathscr{R}$ in the simulation, e.g. run D9.6 is a
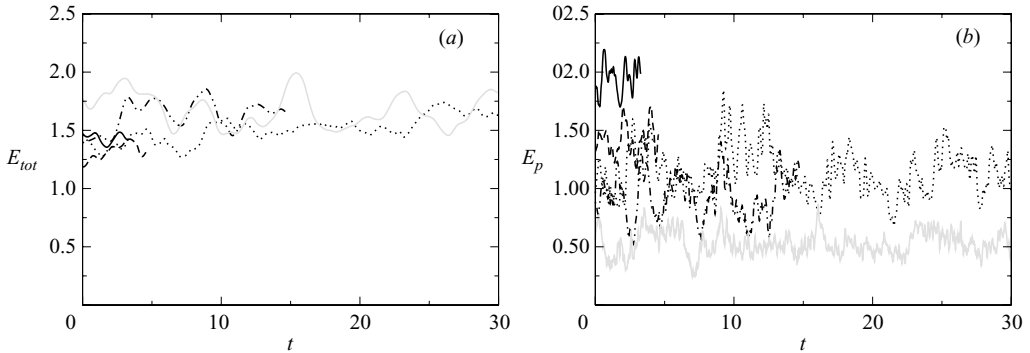
FIGURE 1. The time evolution of (a) the total energy $E_{tot}/(PL_h)^{2/3}$ and (b) the potential energy $E_P/(PL_h)^{2/3}$. ———, B9.3; — — —, B3.0; · · · · ·, B1.1; — · · — · · —, B0.4; grey line, B0.1.

simulation with $\mathscr{R} = 9.6$. Owing to computational limitations, we have only carried out simulations up to $\mathscr{R} \simeq 16$. The root-mean-square of the horizontal velocity fluctuations U is used as the characteristic velocity scale, l_h is estimated as $l_h = U^3/\varepsilon$ and the other parameters as in (2.12). F_h is small and, as a result, $l_v \ll l_h$. Therefore, we set $L_v < L_h$. In all the simulations $Sc = 0.70$ and this corresponds closely to stratified air.

The requirement for the resolution to have well-resolved small scales is $k_{max}\eta > 1$ (de Bruyn Kops & Riley 1998), where k_{max} is the maximum resolved horizontal wavenumber. To reduce the computational costs, the simulations were started with a relatively low resolution. The resolution was then increased in steps to the final resolution listed in table 1 satisfying $k_{max}\eta > 1$. During the beginning of the time series which will be presented the resolution was lower than the final resolution. All statistics which do not include time series are calculated from the final stage with the high resolution.

4. Results

4.1. *Time series and general observations*

In figure 1, time series of the total energy $E_{tot} = E_K + E_P$ and potential energy E_P extracted from the B-runs are plotted after the simulations had reached approximately statistical stationarity. Energy is normalized by $(PL_h)^{2/3}$, where P is the forcing power, and time t is normalized by $(P/L_h^2)^{1/3}$ (also in the figures hereafter). Both E_{tot} and E_P show large fluctuations during the computations, but such fluctuations have also been observed in DNS of forced isotropic turbulence when the forcing is restricted to the lowest modes. Time series of the dissipation $\varepsilon_{tot} = \varepsilon + \varepsilon_P$ and ε_P presented in figure 2 show significant fluctuations as well, but ε_{tot} normalized by P fluctuates about the value 1, implying a balance between dissipation and forcing input on average. Time series of the energy and the dissipation in other runs were similar to the B-runs, e.g. after the transition period the power input is on average balanced by the dissipation and energy remains approximately constant.

Figure 3 shows the evolution of kinetic energy in the shear modes, i.e. $E_K(k_h = 0)$, normalized with the total kinetic energy. The fraction of energy in the shear modes varies but it is significant in all runs. In some runs, the energy in the shear modes does not seem to increase, but in others a slow growth can be observed on a very long time scale, which is not related to any dynamical time scale of the flow. Neither is there any relation between the growth rate and Re or F_h. Such a slow accumulation
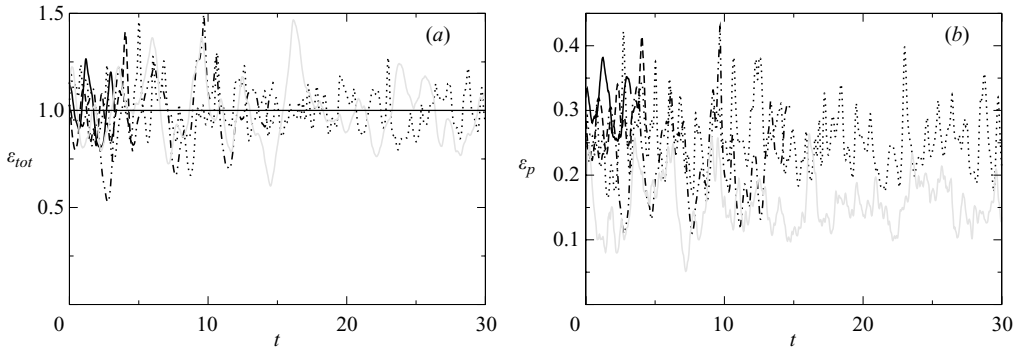
FIGURE 2. The time evolution of (*a*) the total energy dissipation ε_{tot}/P and (*b*) the potential energy dissipation ε_P/P. Lines as in figure 1.
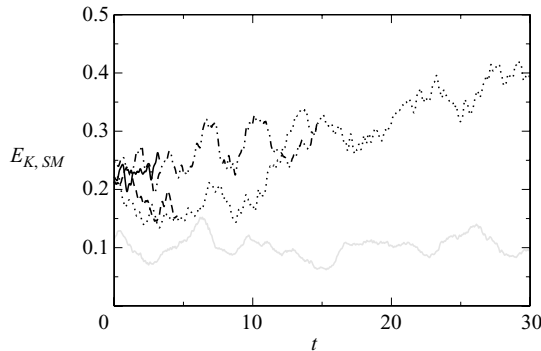

FIGURE 3. The time evolution of $E_K(k_h=0)/E_K$. Lines as in figure 1.

of energy in the shear mode has also been observed by Smith & Waleffe (2002), Laval *et al.* (2003), Waite & Bartello (2004, 2006) and Lindborg (2006). In these studies, it was argued that this could be due to the use of periodic boundary conditions. There is some evidence that this has little or an insignificant influence on the dynamics of the flow and on the quantities of interests (Waite & Bartello 2004; Lindborg 2006). Following Waite & Bartello (2004, 2006) and Lindborg (2006), we do not try to reach a complete equilibrium with respect to the amount of energy in the shear mode because this would be computationally too costly. Hereafter, we consider the flow to be statistically stationary if the energy and the dissipation reach an approximately constant value.

Using the scaling $\rho' \sim U^2 \rho_0/(gl_v)$ presented in §2 together with $l_v \sim U/N$ for $\mathcal{R} \gg 1$ and (2.19) for $\mathcal{R} \ll 1$, we can deduce that $E_P \sim E_K$ when $\mathcal{R} \gg 1$ and $E_P \sim E_K\mathcal{R}$ when $\mathcal{R} \ll 1$. Figure 4(*a*) presents the mean ratios E_P/E_K extracted from the DNS. A general increase of E_P/E_K is observed with increasing $\mathcal{R}$ and the ratio E_P/E_K seems to asymptote to a constant value of about 0.15 when $\mathcal{R} > 1$, in agreement with the scaling predictions. This is quite close to the values computed by Lindborg (2006). The ratio E_P/E_K can be affected by the forcing method, but the trend should be universal in all simulations using the same forcing method. The ratio $\varepsilon_P/\varepsilon$, shown in figure 4(*b*), approaches a constant value of about $0.4 - 0.5$ when $\mathcal{R} > 1$ in agreement with Riley & deBruynKops (2003) and Lindborg (2006). When $\mathcal{R} < 1$, the ratio $\varepsilon_P/\varepsilon$ decreases with decreasing $\mathcal{R}$ as does the ratio E_P/E_K.
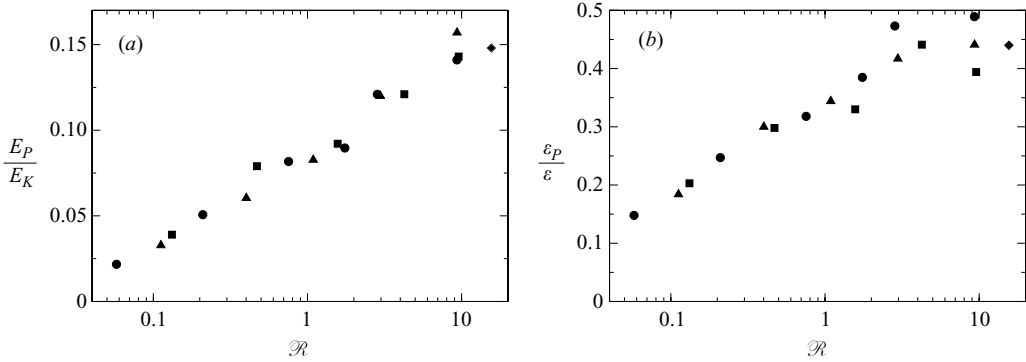
FIGURE 4. The average ratio (*a*) E_P/E_K and (*b*) $\varepsilon_P/\varepsilon$ as a function of $\mathscr{R}$. Circles, runs A;
triangles, runs B; diamond, run C; squares, runs D.

Some additional physical parameters extracted from the DNS are presented in
table 1. We can see that $\langle u'_z u'_z \rangle / E_K$ is small and decreases with decreasing F_h in
agreement with the scaling analysis in §2 which predicts $\langle u'_z u'_z \rangle / E_K \sim F_h^2$ when $\mathscr{R} \gg 1$.
However, this scaling could not strictly be confirmed but it should be noted that
the anisotropy of the turbulence is partly affected by the forcing. The buoyancy flux
correlation $\langle u'_z \rho' \rangle / u'_{z,rms} \rho'_{rms}$ shows that the density fluctuations are in all cases weakly
correlated to the vertical turbulent motions. It can be shown that the present scaling
assumptions for $\mathscr{R} > 1$ predict a finite value for $\langle u'_z \rho' \rangle / u'_{z,rms} \rho'_{rms}$, irrespective of F_h.

4.2. *Flow structures*

In this section, we study the flow structures after the simulations have reached a
statistically stationary state. Snapshots of the fluctuating density field on a vertical
(x, z)-plane extracted from several simulations are presented in figure 5. The ratio
between the horizontal and vertical scales in the figures is the same as in the
simulations. In all simulations visualized in figure 5, $F_h \simeq 0.015$ but Re increases from
bottom to top. The appearance of the density field is strikingly different according to
the snapshots. At relatively low Re and $\mathscr{R} < 1$, the density field is smooth with relatively
flat large-scale structures. No small-scale disturbances are visible and this points to the
significant influence of viscosity on the dynamics. When Re is increased, large-scale
structures remain visible, but small-scale disturbances become more frequent and a
sharper gradient between the large-scale anisotropic structures can be observed in
figure 5, see in particular the snapshot extracted from run D9.6. These disturbances,
presumably caused by the sharp vertical gradients between the large structures, suggest
the existence of Kelvin–Helmholtz instabilities. They can also be the manifestation
of three-dimensional turbulence for scales smaller than l_O in the weakly stratified
range. Kelvin–Helmholtz-type instabilities generated by the intense shear between the
large-scale layers that subsequently break down into three-dimensional turbulent-like
motions were also seen by Riley & deBruynKops (2003).

The features for $\mathscr{R} < 1$ and $\mathscr{R} > 1$ observed in figure 5 can also be seen at other
F_h. Figure 6 shows a vertical slice extracted from run D0.5 with $F_h = 0.0039$ and
$Re = 31\,000$. Smooth but very thin layers can be seen whereas disturbances are almost
absent. The thickness of the layers agrees with scaling relation (2.19) for $\mathscr{R} < 1$ as
will be shown later. Such very smooth layers with apparently no or few small-scale
disturbances were also observed by Waite & Bartello (2004) and Laval *et al.* (2003)
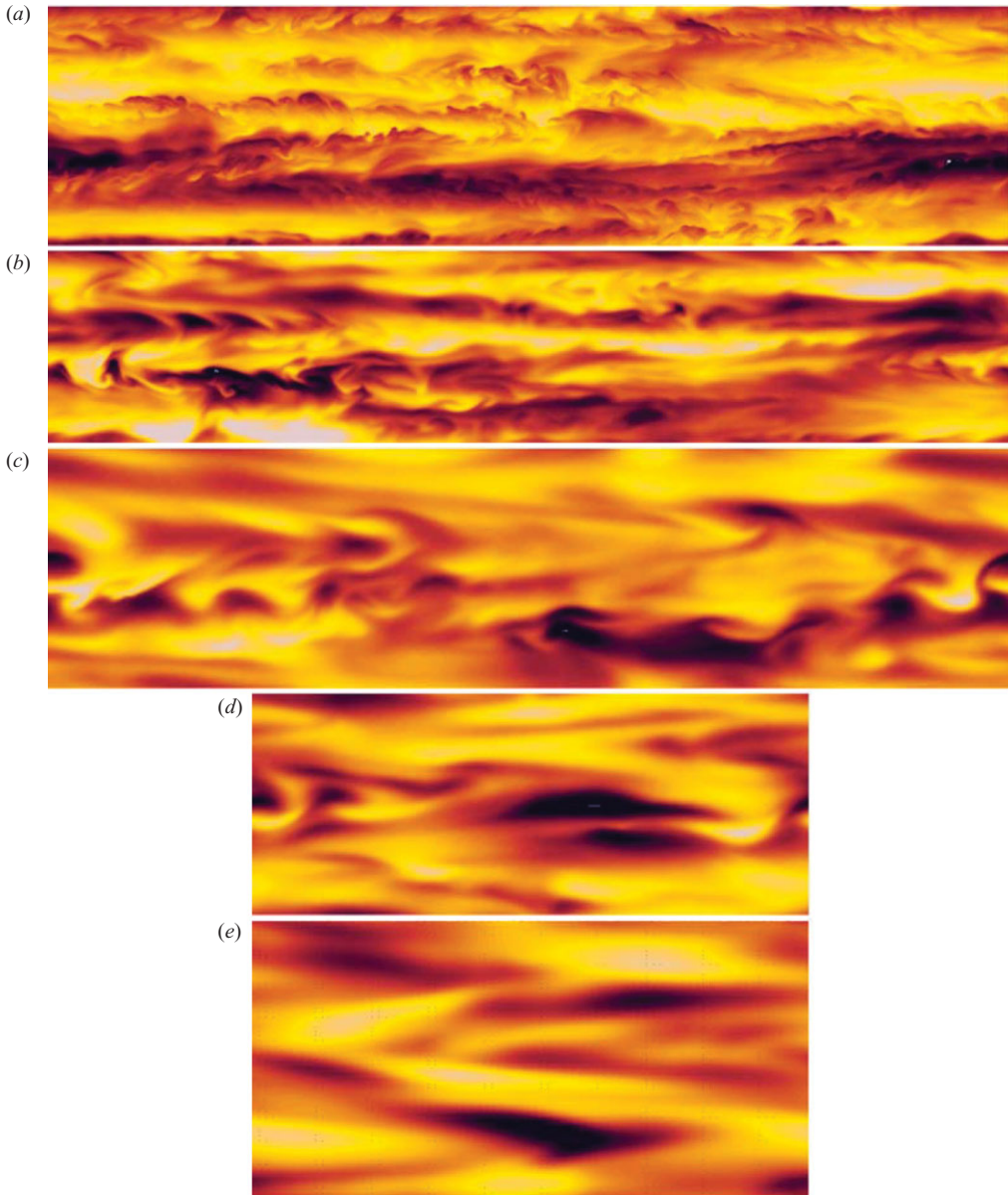at low F_h. Note that the layer formation in the present simulations is entirely the

FIGURE 5. Snapshots of the density fluctuations in a vertical plane for $F_h \simeq 0.015$.
(*a*) run D9.6, (*b*) B3.0, (*c*) A1.8, (*d*) R0.7 and (*e*) R0.3.
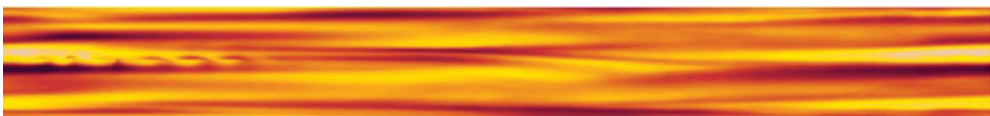

FIGURE 6. Snapshot of the density fluctuations in a vertical plane extracted from run D0.5.

result of dynamical processes in the stratified fluid because the forcing is purely two-dimensional and horizontal. At the start of the simulations, only large, horizontal motions and random perturbations are present in the fluid but the large-scale
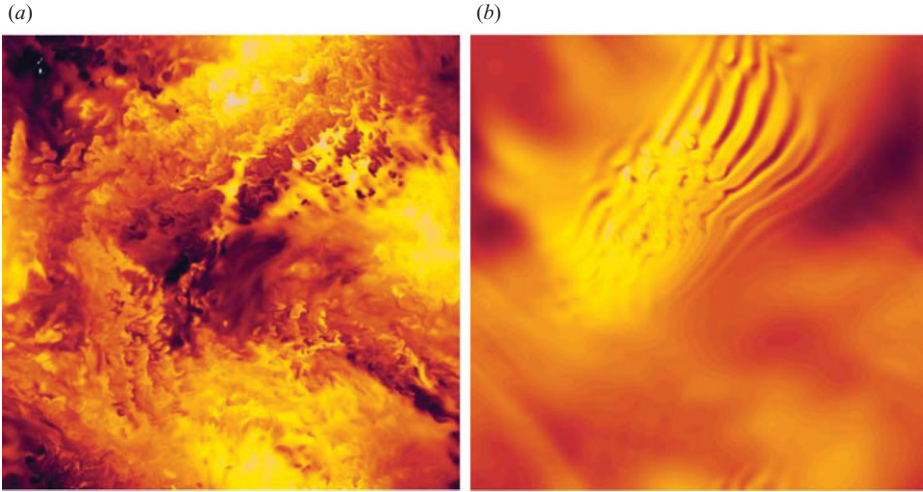
(a)   (b)

FIGURE 7. Snapshot of the density fluctuations in a horizontal plane: (a) run D9.6
and (b) run B0.4.
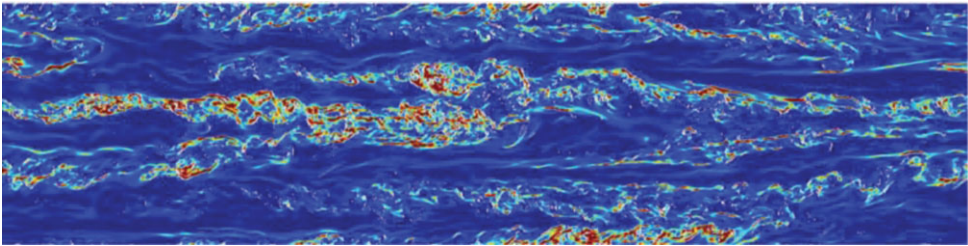
FIGURE 8. Snapshot of ε on an (x, z)-plane extracted from run D9.6. From low to high
dissipation goes from dark blue, light blue to red.

quasi-vertical structures are unstable and layers develop after some time. The
spontaneous layer formation might be the result of the zigzag instability studied
in detail by Billant & Chomaz (2000a).

In figure 7, we show snapshots of the density field on an (x, y)-plane (horizontal
plane). The large-scale structures are the footprints of the large-scale, horizontal
forcing applied in the present simulations. Smaller-scale, turbulent-like motions are
clearly visible at many places in the snapshot when $\mathscr{R} > 1$ (plot a). On the other hand,
when $\mathscr{R} < 1$ (plot b) much of the density field appears to be undisturbed and only
localized wave-like disturbances can be observed in figure 7.

In figure 8, we show a snapshot of the kinetic energy dissipation ε extracted from
run D9.6 on the same plane as in figure 5(a). The small-scale turbulent-like motions
and sharp vertical gradients in the density field appear to correlate with intense
dissipation.

Probability density functions (PDFs) of the local Richardson number

$$Ri = \frac{-(g/\rho_0)(\partial \rho^*/\partial z')}{\frac{1}{2}[(\partial u'_x/\partial z')^2 + (\partial u'_y/\partial z')^2]},$$

where u'_x and u'_y are the two horizontal velocity components and ρ^* is the sum of
the ambient and the fluctuating density field, are presented in figure 9. A negative
Ri signifies overturning of the density field and regions with $Ri < 0.25$ are prone to
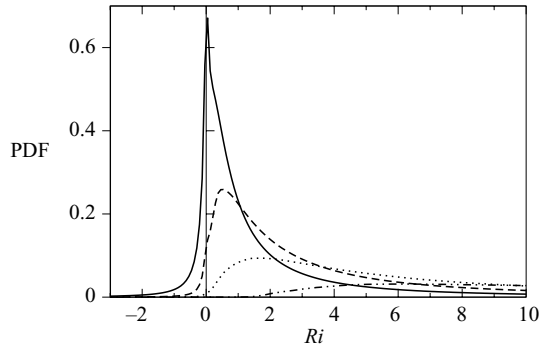
FIGURE 9. PDF of the local Richardson number Ri. ———, D9.6; – – –, D1.6; $\cdots\cdots$, D0.5; $-\cdot\cdot-\cdot\cdot-$, D0.1.
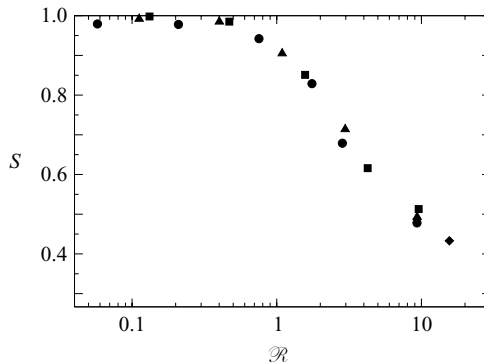

FIGURE 10. The anisotropy S of the dissipation defined by (4.1) as a function of $\mathscr{R}$. Circles, runs A; triangles, runs B; diamond, run C; squares, runs D.

shear instabilities according to the Miles–Howard criterion. From figure 9, it can be deduced that the occurrence of negative Ri and thus overturning of the density field increases when $\mathscr{R}$ increases, in agreement with the visualizations presented in figures 5 and 7. In all cases with $\mathscr{R} < 1$, the probability of negative Ri is small, and is negligible if $\mathscr{R} \ll 1$ confirming the strong stability of the flow with respect to vertical shear instabilities. Furthermore, we see that the PDFs have a peak at $Ri = 0$ when $\mathscr{R} > 1$, implying a high probability of well-mixed regions with a zero total density gradient. This indicates the existence of a step-like density profile: well-mixed regions separated by large and sharp gradients in the density field. Such a step-like profile in the scalar field is a common phenomenon in classical turbulence and stratified turbulence (Park *et al.* 1994). In contrast, when $\mathscr{R} < 1$, the PDFs have no peak at $Ri = 0$ but one at $Ri \simeq \mathscr{R}^{-1}$ as implied by (2.16), showing that most of the density perturbations are suppressed.

In figure 10, the ratio of the dissipation due to vertical shearing and the total dissipation

$$S = \frac{\nu \langle (\partial u'_x/\partial z')^2 + (\partial u'_y/\partial z')^2 \rangle}{\varepsilon} \tag{4.1}$$

is plotted as a function of $\mathscr{R}$. The visualizations have shown that turbulent motions and instabilities are nearly absent if $\mathscr{R} < 1$, suggesting that in this case dissipation of kinetic energy is mainly due to vertical shearing of the layers, and this is confirmed by
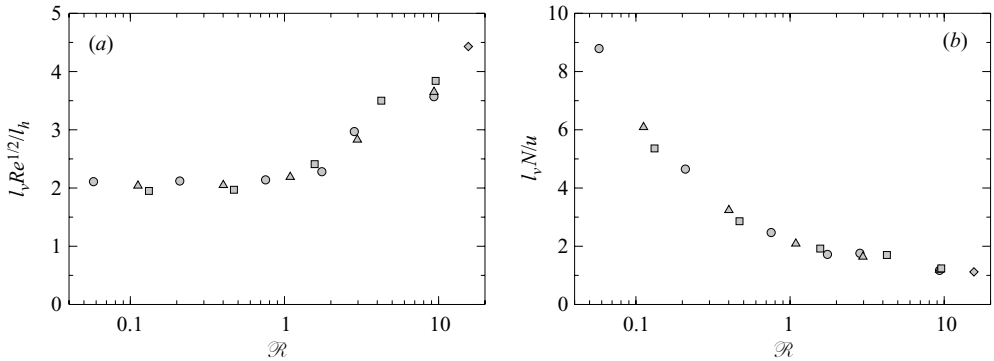
FIGURE 11. The scaled vertical length scale (*a*) $l_v Re^{1/2}/l_h$ and (*b*) $l_v N/U$ as a function of $\mathscr{R}$. Circles, runs A; triangles, runs B; diamond, run C; squares, runs D.

figure 10 because $S \simeq 1$ for $\mathscr{R} < 1$. Praud *et al.* (2005) observed as well the predominant dissipation by vertical shearing for $\mathscr{R} < 1$. Although the forward cascade of energy is very weak for $\mathscr{R} < 1$ as we will show later, the significant dissipation of energy by vertical shearing of the large-scale motions makes a statistically stationary state possible.

When $\mathscr{R} > 1$, a Kolmogorov-like turbulence range develops for horizontal scales smaller than l_O as explained in §2.3, with weak effects of stratification suggesting dissipation of energy by small, approximately isotropic scales. In agreement with this, figure 10 shows that the dissipation becomes more isotropic because S decreases and approaches the value for isotropic turbulence $S = 0.267$ when $\mathscr{R}$ increases. The same dependence of the anisotropy of dissipation on F_h and Re individually have been observed by Riley & deBruynKops (2003) and Waite & Bartello (2004) respectively, but no relation has been established between dissipation characteristics and $\mathscr{R}$. Our results are also consistent with the DNS of stratified mixing layer by Smyth & Moum (2000). They found that the anisotropy of the velocity gradients was determined by the buoyancy Reynolds number $\varepsilon/(\nu N^2)$ when the flow was no longer influenced by the initial conditions. Their simulations showed a large contribution of the vertical shearing of the streamwise velocity component for $\varepsilon/(\nu N^2) < 1$, an approach to isotropy for $\varepsilon/(\nu N^2) > 1$ and a clear transition from the highly anisotropic state to the more isotropic state around $\varepsilon/(\nu N^2) \simeq 1$. These observations have been also qualitatively confirmed by Hebert & de Bruyn Kops (2006).

4.3. *Scales*

The length scales need to be computed to validate the scaling analysis presented in §2. The horizontal length scale l_h, calculated using Taylor's estimate, is mainly determined by the large-scale forcing and is approximately equal to the domain size L_h in all simulations as shown in table 1. The vertical length scale l_v is computed as explained in Appendix B and is much smaller than l_h, as shown in table 1, revealing the strong anisotropy of the large scales and legitimating the use of a stretched domain in our computations. Still, in all simulations, l_v is smaller than the computational domain height L_v so that it contains several layers, as seen for example in figure 6. Since Waite & Bartello (2004) showed that no vertical scales larger than l_v are present in a stratified fluid, it can be claimed that the vertical scales are not confined by the computational domain.
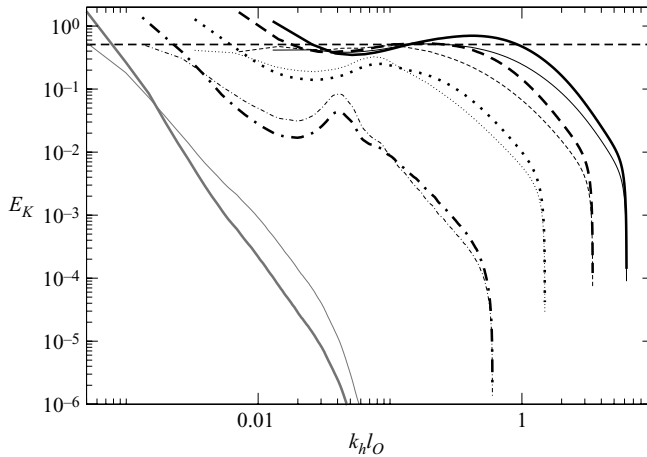
FIGURE 12. The compensated horizontal one-dimensional kinetic energy spectra $E_K(k_h)k_h^{5/3}/\varepsilon_K^{2/3}$ (thick lines) and potential energy spectra $E_P(k_h)k_h^{5/3}\varepsilon_K^{1/3}/\varepsilon_P$ (thin lines). The horizontal wavenumber k_h is scaled by l_O. ———, D9.6; — — —, D4.2; · · · · ·, D1.6; — · · — · · —, D0.5; grey line, D0.1.

In figure 11, l_v scaled by $l_h Re^{-1/2}$ and by U/N is displayed. The vertical length scale extracted from all the different simulations clearly shows the scaling $l_v \sim l_h Re^{-1/2}$ when $\mathcal{R} < 1$ and supports the scaling $l_v \sim U/N$ when $\mathcal{R} > 1$. We stress that the values of l_v display a large scatter without the scalings since the DNS covers a fairly wide range of F_h and Re. Moreover, the scalings show that the transition between the two regimes takes place around $\mathcal{R} = 1$ and are fully consistent with the hypotheses presented in §2. These results can explain why Godeferd & Staquet (2003) observed the scaling $l_v \sim U/N$ because $\mathcal{R} > 1$ in their simulations, whereas Praud *et al.* (2005) observed a scaling consistent with $l_v \sim l_h Re^{-1/2}$ because $\mathcal{R} < 1$ in their experiments.

4.4. *Spectra*

The one-dimensional vertical and horizontal spectra studied here are computed in the same way as in Lindborg (2006). In figure 12, compensated horizontal one-dimensional kinetic energy spectra $E_K(k_h)k_h^{5/3}/\varepsilon_K^{2/3}$ and potential energy spectra $E_P(k_h)k_h^{5/3}\varepsilon_K^{1/3}/\varepsilon_P$ extracted from the D-runs are shown. The spectra are compensated according to (2.17) and the value obtained by Lindborg (2006) for $C_1 \simeq C_2 = 0.51$ is represented by the straight line in figure 12. The hypothesis presented in §2.3 for $\mathcal{R} \gg 1$ predicts a stratified turbulence inertial range with a $k_h^{-5/3}$-power-law behaviour for $k_h l_O \ll 1$. We do not see such a clear range in our simulations because $\mathcal{R}$ is presumably not large enough in the DNS to have an inertial range virtually free of viscous effects. Moreover, the wavenumber band with an eventual inertial range is small in the DNS, hindering the assessment of power-law behaviour. Nevertheless, the spectra extracted from runs D9.6 and D4.2 show a wavenumber range close to the straight line, suggesting an approach to the $k_h^{-5/3}$-power-law behaviour, but a plateau in the compensated spectra as in the simulations of Lindborg (2006) using hyperviscosity is not clearly discernible. The spectra extracted from run D9.6 show a 'bump' at higher k_h. This bump is probably caused by Kelvin–Helmholtz instabilities generating more classical three-dimensional turbulence at small scales. Such a 'bump' was observed by Lindborg (2006) as well at moderate Re. The slope of the spectra at the lowest wavenumbers is a consequence of the forcing. The compensated kinetic energy spectra
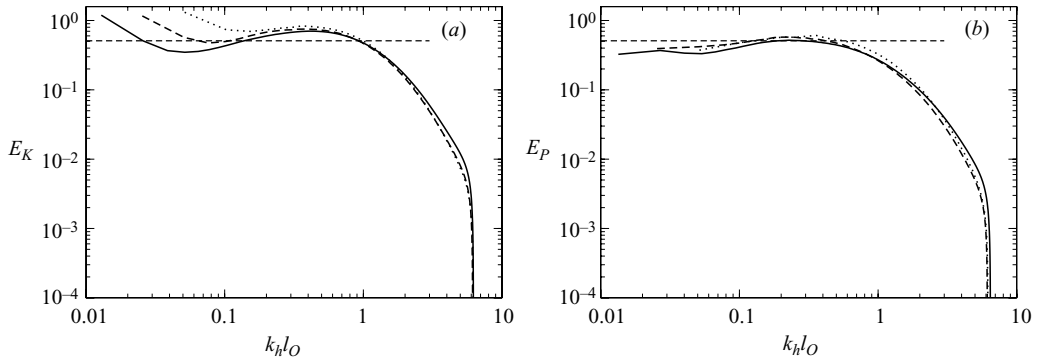
FIGURE 13. The compensated horizontal one-dimensional (*a*) kinetic energy spectra $E_K(k_h)k_h^{5/3}/\varepsilon_K^{2/3}$ and (*b*) potential energy spectra $E_P(k_h)k_h^{5/3}\varepsilon_K^{1/3}/\varepsilon_P$ at $\mathscr{R} \simeq 9$. The horizontal wavenumber k_h is scaled by l_O. ———, D9.6; — — —, B9.3; $\cdots\cdots$, A9.3.

and the potential energy spectra approximately overlap each other at intermediate wavenumbers when $\mathscr{R} > 1$, giving support to the hypothesis of Lindborg (2006) that these spectra have the same form and the finding that $C_1 \simeq C_2$. The differences between the kinetic and potential energy spectra at low wavenumbers is caused by the forcing whereas the differences at high wavenumbers might be related to the non-unity Schmidt number used in our DNS ($Sc = 0.7$).

Spectra extracted from the simulations with $\mathscr{R} < 1$ deviate significantly from the others. The spectra have a steep slope and there is obviously no wavenumber range that resembles a $k_h^{-5/3}$-power-law range. Spectra extracted from runs D1.6 and D0.5 display a distinct peak. This is probably a fingerprint of the intermittent shear instabilities observed in visualizations (figure 6) and also revealed by PDFs of the local Richardson number in these cases (figure 9). Such peaks in the spectra were also observed by Laval *et al.* (2003) when shear instabilities were present in the flow. The kinetic energy spectrum extracted from run D0.1 is very steep with a slope close to k_h^{-5}, which bears close similarities with the spectra obtained by Laval *et al.* (2003) and Waite & Bartello (2004) in the most strongly stratified cases.

Compensated horizontal kinetic and potential energy spectra extracted from runs A9.3, B9.3 and D9.6 are displayed in figure 13. In all three simulations, $\mathscr{R} \simeq 9$, but Re and F_h are varying. According to (2.13), the width of the inertial range should increase as $F_h^{-3/2}$ toward low $k_h l_O$, and we see a broadening of the plateau with decreasing F_h, which is in qualitative agreement with (2.13). However, the inertial range is not sufficiently well-defined to make a quantitative comparison, but nevertheless the spectra appear to confirm the scaling suggested by (2.17) and show that the parameter determing the shape of the spectrum is neither F_h nor Re but $\mathscr{R}$.

Figure 14 displays compensated spectra for three simulations with $\mathscr{R} \simeq 0.1$ but different Re and F_h. In all cases the spectra are very steep and different from those in figure 13. This supports the hypothesis that when $\mathscr{R} < 1$ turbulent inertial-range dynamics does not exist, irrespectively of the value of Re.

Following Lindborg (2006), we define the kinetic energy flux through a certain horizontal wavenumber k_ρ as

$$\Pi_K(k_\rho) = -\sum_{k_v} \sum_{\sqrt{k_x^2+k_y^2} \leqslant k_\rho} T_K(k_x, k_y, k_v), \qquad (4.2)$$
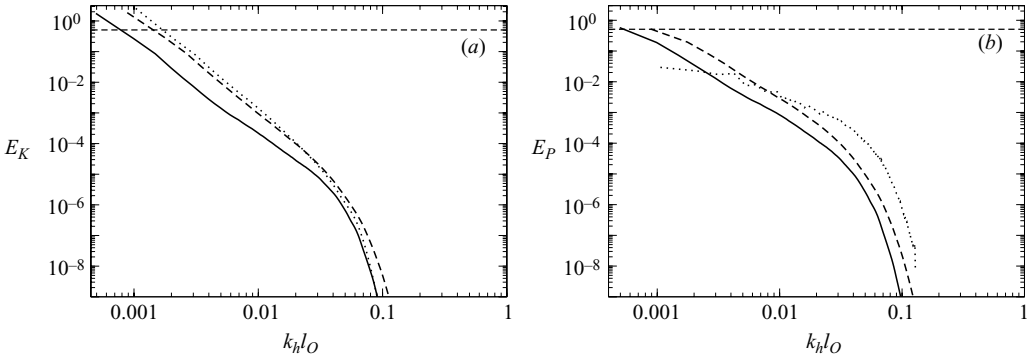
FIGURE 14. The compensated horizontal one-dimensional (*a*) kinetic energy spectra $E_K(k_h)k_h^{5/3}/\varepsilon_K^{2/3}$ and (*b*) potential energy spectra $E_P(k_h)k_h^{5/3}\varepsilon_K^{1/3}/\varepsilon_P$ at $\mathcal{R} \simeq 0.1$. The horizontal wavenumber k_h is scaled by l_O. ———, D0.1; $---$, B0.1; $\cdots\cdots$, A0.06.
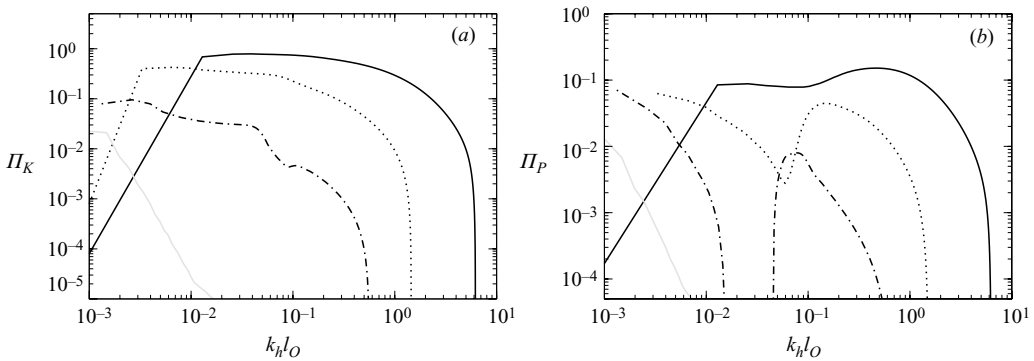

FIGURE 15. The horizontal (*a*) kinetic energy flux $\Pi_K(k_h)$ and (*b*) potential energy flux $\Pi_P(k_h)$. ———, D9.6; $\cdots\cdots$, D1.6; $-\cdot-\cdot-$, D0.5; grey line, D0.1.

where T_k is the spectral energy transfer function (see Lindborg 2006). The flux of potential energy, $\Pi_P(k_\rho)$, is defined in the corresponding way. A positive energy flux $\Pi_K(k_\rho)$ or $\Pi_P(k_\rho)$ implies a net transfer of energy from large to small scales and a negative flux implies an inverse cascade. Figure 15 shows $\Pi_K(k_\rho)$ and $\Pi_P(k_\rho)$. The data extracted from run D9.6 show that Π_K is positive, which is a clear manifestation of an energy flux from large to small scales. Furthermore, a range of scales where Π_K is approximately constant is visible and this points to the emergence of an inertial subrange. When $\mathcal{R}$ decreases, this inertial subrange with an approximately constant Π_K disappears progressively. When $\mathcal{R} < 1$, the flux remains positive, but Π_K decreases rapidly for large k_h, implying that the transfer of energy from large to small scales is weak. A clear transfer of potential energy from large to small scales is noticeable in the energy flux extracted from run D9.6 as shown in figure 15(*b*). In the range $0.01 < k_\rho l_O < 0.1$, Π_P is approximately constant, but the energy flux increases when $k_h l_O$ increases to 0.5. This 'bump' appears at the same wavenumbers as the 'bump' in the compensated energy spectra. The potential energy flux is also positive in run D1.6, but the flux has a clear 'dip' with a decreased energy flux around $k_\rho l_O \simeq 0.06$, implying a disruption of the flux from large to small scales. In run D0.5, Π_P is even negative between $k_\rho l_O = 0.012$ and 0.045, implying a net, but small, potential energy flux from small to large scales in this wavenumber range. Accordingly, computed energy
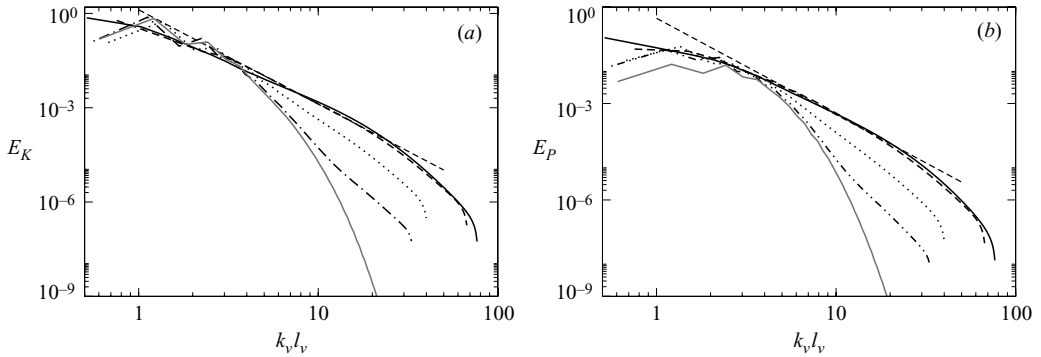
FIGURE 16. The vertical (a) kinetic energy spectra $E_K(k_v)/(U^2 l_v)$ and (b) potential energy spectra $E_P(k_v)/(U^2 l_v)$. $k_v l_v$ is the vertical wavenumber scaled with the vertical length scale l_v. Lines as in figure 12. The straight dashed line has a slope k^{-3}.
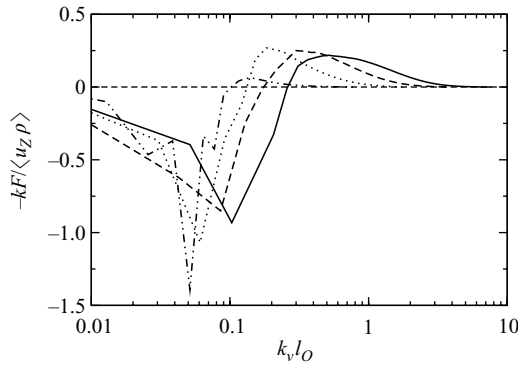

FIGURE 17. The scaled vertical buoyancy flux spectrum $-k_v F(k_v)/\langle u_z' \rho' \rangle$. The vertical wavenumber is scaled by l_O. Lines as in figure 12.

dissipation spectra (results not shown) reveal that in this run most of the energy is dissipated by large horizontal scales at wavenumbers near the forced wavenumbers whereas in run D9.6 the major fraction is dissipated by small-scale motions.

   Vertical spectra of kinetic and potential energy are displayed in figure 16. Both spectra are scaled by $U^2 l_v$ and vertical wavenumbers are scaled by l_v. The slope of the spectra for $\mathcal{R} > 1$ is close to or slightly less steep than k_v^{-3} for intermediate wavenumbers and is consistent with the similarity form (2.18). In contrast, the vertical spectra for $\mathcal{R} < 1$ do not reveal any power-law range and are steeper than k_v^{-3} at high wavenumbers.

   In figure 17, vertical co-spectra $F(k_v)$ of the vertical buoyancy flux $u_z' \rho'$ are shown. The spectra are multiplied by k_v to accentuate the high-wavenumber behaviour and scaled by $\langle u_z' \rho' \rangle$. A positive $F(k_v)$ (implying a negative $-k_v F(k_v)/\langle u_z' \rho' \rangle$ displayed in the figure) corresponds to down-gradient buoyancy flux and a conversion of kinetic into potential energy. A positive sign in the figure implies a counter-gradient flux: displaced fluid parcels move back to their equilibrium position and the fluid is said to re-stratify (Holloway 1988; Staquet & Godeferd 1998). At low k_v, the spectrum in all displayed simulations is negative meaning a transfer from kinetic to potential energy at large scales. Note that the current forcing method whereby only the horizontal velocity field is forced imposes $\langle u_z' \rho' \rangle \geqslant 0$ (this follows from the balance equation

of the potential energy), but it does not directly force u'_z and hence the buoyancy flux. However, at higher k_v the co-spectra are positive, implying a re-stratification at vertical scales near the Ozmidov scale. These counter-gradient fluxes are significant and particularly evident when $\mathcal{R} > 1$. In run D9.6 the integrated counter-gradient flux normalized by the total flux is 0.25 for example. Counter-gradient buoyancy fluxes at small scales were observed by Holloway (1988), Staquet & Godeferd (1998) and Carnevale, Briscolini & Orlandi (2001). Holloway also studied the issue theoretically. The re-stratification at small vertical scales coincides with the existence of shear instabilities, overturning motions and small-scale turbulence existing for $\mathcal{R} > 1$ as shown in §4.2. In run D0.5, where there are virtually no small-scale turbulent motions, the counter-gradient flux is negligible, but in run D9.6, counter-gradient fluxes are important which goes hand-in-hand with the appearance of Kelvin–Helmholtz-type instabilities and turbulent-like small-scale motions in the fluid.

5. Discussion

The scaling analysis presented in §2 has been validated through a series of DNS of homogeneous turbulence with strong stratification and a purely horizontal forcing of the large horizontal velocity scales. Re and F_h have been varied in the DNS so that the dynamics in the two distinct regimes $\mathcal{R} > 1$ and $\mathcal{R} < 1$ could be investigated.

After a transition period, the flow attained a statistically stationary or quasi-stationary state in all simulated cases, with an approximately constant mean kinetic and potential energy and a forcing energy input on average balanced by the dissipation. Visualizations revealed significant differences between the simulations with $\mathcal{R} > 1$ and $\mathcal{R} < 1$ respectively. When $\mathcal{R} < 1$, large smooth and stable horizontal layers were observed which were thin at high Re. Occasionally, some local wave-like disturbances were seen but turbulent-like structures were usually absent. On the other hand, when $\mathcal{R} > 1$ large quasi-horizontal layers were still noticeable but at the same time disturbances resembling Kelvin–Helmholtz-type rollers and smaller-scale three-dimensional turbulent-like motions were abundantly present in the flow. We have argued that scales below l_O were weakly affected by stratification. Correspondingly, the small-scale dissipation approached isotropy when $\mathcal{R} > 1$ whereas the dissipation was predominantly due to vertical shearing when $\mathcal{R} < 1$. Other statistics extracted from the DNS, such as the ratio of potential to kinetic energy, revealed clear differences in the regimes $\mathcal{R} < 1$ and $\mathcal{R} > 1$ as well. Moreover, several statistics displayed an approximately universal behaviour in terms of $\mathcal{R}$, confirming the importance of this parameter for the dynamics of stratified flows.

Horizontal and vertical kinetic and potential energy spectra were extracted from the DNS. When $\mathcal{R} < 1$ the horizontal spectra were very steep whereas for $\mathcal{R} > 1$ the spectra displayed a wavenumber range that approached a $k_h^{-5/3}$-power-law behaviour, in accordance with the studies of Riley & deBruynKops (2003) and Lindborg (2006). When $\mathcal{R} > 1$ vertical spectra were steeper than the horizontal spectra and approximated k_v^{-3}. Most of the energy was dissipated by relatively large horizontal scales when $\mathcal{R} < 1$ whereas for $\mathcal{R} > 1$ a significant fraction was dissipated at small scales which signified an energy transfer from large to small scales. This was confirmed by computed energy flux spectra which showed a clear energy cascade from large to small scales and the appearance of an inertial range when $\mathcal{R} > 1$. On the other hand, the spectral energy flux was very weak when $\mathcal{R} < 1$, implying that the energy is mainly dissipated by vertical shearing at scales close to the forcing scales.
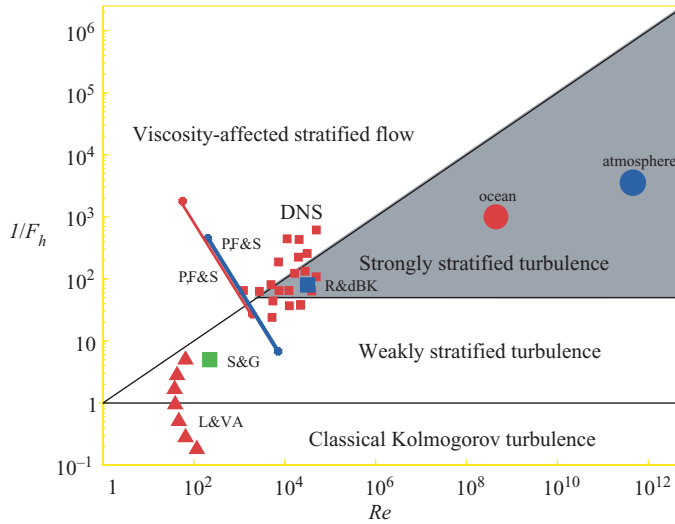
FIGURE 18. Regimes in stably stratified flows. The conditions under which our and other DNS and experiments are carried out are represented by symbols. Red squares (labelled DNS): present DNS; blue square (R&dBK): DNS run F4R64 by Riley & deBruynKops (2003); green square (S&G): DNS run A by Staquet & Godeferd (1998); red triangles (L&VA): experiment of decaying stratified turbulence by Lienhard & Van Atta (1990) listed in their table 1; red and blue lines (P,F&S): experiments bc and be of decaying stratified turbulence by Praud *et al.* (2005). Conditions typically found in the middle atmosphere (Lindborg 2006) and the upper ocean (Moum 1996) are shown by the blue and red circle respectively, but these conditions can vary considerably. Values of Re and F_h are estimated using (2.12).

Many observations in other studies on stratified flows are in accordance with our observations at either $\mathscr{R} < 1$ or $\mathscr{R} > 1$. The smooth, elongated horizontal and nearly undisturbed layers with strong viscous shearing between them and the very steep horizontal spectra we found when $\mathscr{R} < 1$ correspond to the observations by Laval *et al.* (2003), Waite & Bartello (2004) and Praud *et al.* (2005), whereas the Kelvin–Helmholtz-type instabilities, small-scale turbulent-like motions and the spectra with an approximate $k_h^{-5/3}$-power-law range we found when $\mathscr{R} > 1$ correspond to the observations by Riley & deBruynKops (2003) and Lindborg (2006). The significance of the present study is mainly the series of DNS of stratified turbulence covering a relatively wide range Re and F_h. These simulations strongly support the hypothesis that the two different types of dynamics observed in our and previous studies can be explained by differences only in the parameter $\mathscr{R}$.

We can conclude from these observations that only when $\mathscr{R} = ReF_h^2 > 1$ does a clear and significant transfer of kinetic and potential energy from large to small (horizontal) scales exist and an inertial range emerges with a $k_h^{-5/3}$-power-law behaviour. The scaling analysis was carried out for $\mathscr{R} \to \infty$ but the results from the simulations show that $\mathscr{R} \gtrsim 1$ is already sufficient to observe the features of strongly stratified turbulence. However, we have argued that $\mathscr{R} \gg 1$ is required to have a clear stratified turbulence inertial range. When $\mathscr{R} < 1$, the dynamics (energy transfer, buoyancy flux and dissipation) is predominantly confined to the scales near or at which the energy is injected.

To conclude, figure 18 presents a diagram with the different regimes that are found in stably stratified flows depending on the value of Re and F_h as suggested by this study. The strongly stratified turbulence regime is bounded by the thresholds $\mathscr{R} = ReF_h^2 > 1$ and $F_h < 0.02$, but it should be emphasized that the latter condition

is merely an estimate (Lindborg 2006). When $\mathscr{R} < 1$, we find the viscosity-affected stratified flow regime with large, stable and quasi-two-dimensional layers with strong vertical viscous shearing. For geophysical flows, the strongly stratified turbulence regime is arguably of much interest. This is highlighted in figure 18, which shows that the typical conditions found in the middle atmosphere and the upper ocean fall well inside the strongly stratified turbulence regime. However, this regime is hard to achieve in laboratory experiments and numerical simulations because both a low F_h and a high Re are required. In particular, at moderately high Re, the F_h range where strongly stratified turbulence is found is limited. The diagram shows the conditions under which the DNS have been performed. Some of the present simulations have just met the conditions $Re F_h^2 > 1$ and $F_h < 0.02$ but, unfortunately, with the present computer capacities it is not yet possible to simulate stratified turbulence with $F_h \ll 1$ and at the same time $\mathscr{R} = Re F_h^2 \gg 1$ so that there is a clear inertial subrange with negligible viscous influences. Other DNS and experiments on stratified flows are also displayed in the figure, showing that most of those have been performed under conditions that fall outside the strongly stratified turbulence regime, hence clarifying the differences in the results. The exception is the DNS by Riley & deBruynKops (2003) who carried out DNS at similar values of Re and F_h as in our DNS as seen in the figure, explaining the strong similarities found in our and their simulations.

Further experiments or numerical simulations at higher Re and lower F_h are of importance to study in more detail the dynamics in the regime of strongly stratified turbulence, but this poses a severe challenge. It is also of interest to apply different forcings to investigate if strongly stratified turbulence is a universal phenomenon which is independent of the particular method of energy input at large scales. Interesting possibilities are forcings having a vertical component (in this study we only consider the particular case of purely horizontal forcing) and randomly forced internal waves *vs.* vortical motions. The latter point has been addressed by Waite & Bartello (2004, 2006) and Lindborg & Brethouwer (2007).

Appendix A. Condition for inertial-range stratified turbulence with hyperviscosity

In the same way that we estimated the ratio between large-scale dissipation and total dissipation in (2.15) for Navier–Stokes viscosity we can estimate this ratio when the Navier–Stokes diffusion operator $\nu\nabla^2$ is replaced by a hyperdiffusion operator $(-1)^{n-1}\nu^{(n)}\nabla^{2n}$, where $\nu^{(n)}$ is the hyperviscosity. Assuming that $l_v \sim U/N$ we obtain

$$\frac{\varepsilon_{Large}}{\varepsilon} \sim \frac{\nu^{(n)}\dfrac{\partial^n u}{\partial z^n}\dfrac{\partial^n u}{\partial z^n}\bigg|_{Large}}{\varepsilon} \sim \frac{\nu^n N^{2n} u^{2-2n}}{\varepsilon} = \left(\frac{\eta^{(n)}}{l_O}\right)^{(6n-2)/3} F_h^{n-1}, \qquad \text{(A 1)}$$

where F_h is defined in (2.12) and

$$\eta^{(n)} = \left(\frac{\nu^{(n)}}{\varepsilon^{1/3}}\right)^{3/(6n-2)} \qquad \text{(A 2)}$$

is the generalized Kolmogorov scale. With hyperviscosity the condition for stratified turbulence displaying an inertial range is thus

$$\left(\frac{l_O}{\eta^{(n)}}\right)^{(6n-2)/3} F_h^{1-n} \gg 1. \tag{A 3}$$

In a simulation we should resolve $\eta^{(n)}$. If $F_h \ll 1$ and $n > 1$, this can be accomplished without violating the condition (A 3) even with a resolution scale which is of the order of the Ozmidov length scale or even a little larger. Using (2.13) the condition (A 3) can also be formulated as

$$\frac{l_v}{\eta^{(n)}} \gg F_h^{-1/(3n-1)}. \tag{A 4}$$

For small but finite F_h and very high-order hyperviscosity ($n \to \infty$), the right-hand side is of the order of unity, and in this case it is therefore sufficient that the resolution scale is considerably smaller than $l_v \sim U/N$.

Appendix B. Definition of the vertical length scale

Assume that the vertical kinetic energy spectrum can be written in similarity form as

$$E_K(k_v) = l_v U^2 \tilde{E}(k_v l_v), \tag{B 1}$$

where $\tilde{E}$ is a non-dimensional function. Assume also that $E_K(k_v) \to 0$ faster than $k_v^{-(m+1)}$ as $k_v l_v \to \infty$ and $m > 0$. Then we find

$$\left[\frac{\int_0^\infty E_K(k_v)\,\mathrm{d}k_v}{\int_0^\infty k_v^m E_K(k_v)\,\mathrm{d}k_v}\right]^{1/m} = l_v \left[\frac{\int_0^\infty \tilde{E}(\tau)\,\mathrm{d}\tau}{\int_0^\infty \tau^m \tilde{E}(\tau)\,\mathrm{d}\tau}\right]^{1/m}. \tag{B 2}$$

This relation means that l_v can be calculated from the left-hand side of (B 2), apart from a constant numerical factor. In order to validate a scaling relation such as $l_v \sim U/N$ a constant factor is of no importance. Given the similarity assumption (B 1) we can therefore choose the left-hand side of (B 2) as the definition of l_v, provided that the integral in the denominator converges. We make the choice $m = 1$, which requires that $E_K(k_v)$ falls off faster than k_v^{-2} for large $k_v l_v$. This condition will be satisfied if the spectrum falls off as k_v^{-3}, which we expect it to do in stratified turbulence. The choice $m = 2$ defines the classical Taylor microscale used by Riley & deBruynKops (2003). This choice is more problematic from a theoretical point of view, because it puts too much weight on the small scales, and will therefore be dependent on the Reynolds number. If there exists a broad inertial subrange of Kolmogorov turbulence our choice $m = 1$ would also cause problems since the integral in the denominator of (B 2) would be dominated by this range. In such a case we would have to replace ∞ with the Ozmidov wavenumber $k_O = 1/l_O$ as the upper integration limit, as suggested by Lindborg (2006), but in the present study this is not necessary.

REFERENCES

ALVELIUS, K. 1999 Random forcing of three-dimensional homogeneous turbulence. *Phys. Fluids* **11**, 1880–1889.

BASAK, S. & SARKAR, S. 2006 Dynamics of a stratified shear layer with horizontal shear. *J. Fluid Mech.* **568**, 19–54.

BILLANT, P. & CHOMAZ, J.-M. 2000a Experimental evidence for a new instability of a vertical columnar vortex pair in a strongly stratified fluid. *J. Fluid Mech.* **418**, 167–188.

BILLANT, P. & CHOMAZ, J.-M. 2000b Theoretical analysis of the zigzag instability of a vertical columnar vortex pair in a strongly stratified fluid. *J. Fluid Mech.* **419**, 29–63.

BILLANT, P. & CHOMAZ, J.-M. 2001 Self-similarity of strongly stratified inviscid flows. *Phys. Fluids* **13**, 1645–1651.

DE BRUYN KOPS, S. M. & RILEY, J. J. 1998 Direct numerical simulation of laboratory experiments in isotropic turbulence. *Phys. Fluids* **10**, 2125–2127.

CARNEVALE, G. F., BRISCOLINI, M. & ORLANDI, P. 2001 Buoyancy- to inertial-range transition in forced stratified turbulence. *J. Fluid Mech.* **427**, 205–239.

CHO, J. Y. N. & LINDBORG, E. 2001 Horizontal velocity structure functions in the upper troposphere and lower stratosphere 1. Observations. *J. Geophys. Res.* **106** (D10), 10223–10232.

COT, C. 2001 Equatorial mesoscale wind and temperature fluctuations in the lower atmosphere. *J. Geophys. Res* **106** D2, 1523–1532.

DEWAN, E. M. 1979 Stratospheric spectra resembling turbulence. *Science* **204**, 832–835.

DEWAN, E. M. 1997 Saturated-cascade similitude theory of gravity wave spectra. *J. Geophys. Res* **102** D25, 29, 799-817.

DEWAN, E. M. & GOOD, R. E. 1986 Saturation and the 'universal' spectrum for vertical profiles of horizontal scalar winds in the atmosphere. *J. Geophys. Res* **91**, 2742–2748.

GAGE, K. S. 1979 Evidence for a $k^{-5/3}$ law inertial range in mesoscale two-dimensional turbulence. *J. Atmos. Sci.* **36**, 1950–1954.

GARGETT, A. E., OSBORN, T. R. & NASMYTH, P. W. 1984 Local isotropy and the decay of turbulence in a stratified fluid. *J. Fluid Mech.* **144**, 231–280.

GODEFERD, F. S. & CAMBON, C. 1994 Detailed investigation of energy transfers in homogeneous stratified turbulence. *Phys. Fluids* **6**, . 2084–2100.

GODEFERD, F. S. & STAQUET, C. 2003 Statistical modelling and direct numerical simulations of decaying stably stratified turbulence. Part 2. Large-scale and small-scale anisotropy. *J. Fluid Mech.* **486**, 115–159.

GODOY-DIANA, R., CHOMAZ, J.-M. & BILLANT, P. 2004 Vertical length scale selection for pancake vortices in strongly stratified viscous fluids. *J. Fluid Mech.* **504**, 229–238.

HEBERT, D. A. & DE BRUYN KOPS, S. M. 2006 Relationship between vertical shear rate and kinetic energy dissipation rate in stably stratified flows. *Geophys. Res. Lett.* **33**, L06602.

HERRING, J. R. & MÉTAIS, O. 1989 Numerical experiments in forced stably stratified turbulence. *J. Fluid Mech.* **202**, 97–115.

HINES, C. O. 1991 The saturation of gravity waves in the middle atmosphere. Part I: Critique of linear-instability theory. *J. Atmos. Sci.* **48**, 1348–1359.

HOLFORD, J. M. & LINDEN, P.F. 1999 Turbulent mixing in stratified fluid. *Dyn. Atmos. Oceans* **30**, 173–198.

HOLLOWAY, G. 1988 The buoyancy flux from internal gravity wave breaking. *Dyn. Atmos. Oceans* **12**, 107–125.

KITAMURA, Y. & MATSUDA, Y. 2006 The k_h^{-3} and $k_h^{-5/3}$ energy spectra in stratified turbulence. *Geophys. Res. Lett.* **33**, L05809.

LAVAL, J.-P., MCWILLIAMS, J. C. & DUBRULLE, B. Forced stratified turbulence: Successive transitions with Reynolds number. *Phys. Rev.* E **68**, 036308.

LIENHARD, J. H. & VAN ATTA, C. W. 1990 The decay of turbulence in thermally stratified flow. *J. Fluid Mech.* **210**, 57–112.

LILLY, D. K. 1983 Stratified turbulence and the mesoscale variability of the atmosphere. *J. Atmos. Sci.* **40**, 749–761.

LILLY, D. K., BASSETT, G., DROEGEMEIER, K. & BARTELLO, P. 1998 Stratified turbulence in the atmospheric mesoscales. *Theor. Comput. Fluid Dyn.* **11**, 139–153.

LINDBORG, E. 2002 Strongly stratified turbulence: a special kind of motion. *Advances in Turbulence IX, Proc. Ninth European Turbulence Conference, Southampton.*

LINDBORG, E. 2005 The effect of rotation on the mesoscale energy cascade in the free atmosphere. *Geophys. Res. Lett.* **32**, L01809.

LINDBORG, E. 2006 The energy cascade in a strongly stratified fluid. *J. Fluid Mech.* **550**, 207–242.

LINDBORG, E. & BRETHOUWER G. 2007 Stratified turbulence forced in rotational and divergent modes. *J. Fluid Mech.* (in press).

LINDBORG, E. & CHO, J. Y. N. 2001 Horizontal velocity structure functions in the upper troposphere and lower stratosphere 2. Theoretical considerations. *J. Geophys. Res.* **106** (D10), 10223–10232.

LUMLEY, J. L. 1964 The spectrum of nearly inertial turbulence in a stably stratified fluid. *J. Atmos. Sci.* **21**, 99–102.

MAJDA, A. J. & SHEFTER, M. G. 1998 Elementary stratified flows with instability at large Richardson number. *J. Fluid Mech.* **376**, 319–350.

MÉTAIS, O., BARTELLO, P., GARNIER, E., RILEY, J. J. & LESIEUR, M. 1996 Inverse cascade in stably stratified rotating turbulence. *Dyn. Atmos. Oceans* **23**, 193–203.

MOUM, J. 1996 Energy-containing scales of turbulence in the ocean thermocline. *J. Geophys. Res.* **101**, 14095.

NASTROM, G. D. & GAGE, K. S. 1985 A climatology of atmospheric wavenumber spectra of wind and temperature observed by commercial aircraft. *J. Atmos. Sci.* **42**, 950-960.

PARK, Y.-G., WHITEHEAD, J. A. & GNANADESKIAN, A. Turbulent mixing in stratified fluids: layer formation and energetics. *J. Fluid Mech.* **279**, 279–311.

PRAUD, O., FINCHAM, A. M. & SOMMERIA, J. 2005 Decaying grid turbulence in a strongly stratified fluid. *J. Fluid Mech.* **522**, 1–33.

RILEY, J. J. & DEBRUYNKOPS, S. M. 2003 Dynamics of turbulence strongly influenced by buoyancy. *Phys. Fluids* **15**, 2047–2059.

RILEY, J. J. & LELONG, M.-P. 2000 Fluid motion in the presence of strong stable stratification. *Annu. Rev. Fluid Mech.* **32**, 613–657.

RILEY, J. J., METCALFE, R. W. & WEISMANN, M. A. 1981 Direct numerical simulations of homogeneous turbulence in density stratified fluids. in *Proc. AIP Conf. on Nonlinear Properties of Internal Waves*, pp. 79–112. AIP, Woodbury.

SHIH, L. H., KOSEFF, J. R., IVEY, G. N. & FERZIGER, J. H. 2005 Parameterization of turbulent fluxes and scales using homogeneous sheared stably stratified turbulence simulations. *J. Fluid Mech.* **525**, 193–214.

SMITH, L. M. & WALEFFE, F. 2002 Generation of slow large scales in forced rotating stratified turbulence. *J. Fluid Mech.* **451**, 145–168.

SMYTH, W. D. & MOUM, J. N. 2000 Anisotropy of turbulence in stably stratified mixing layers. *Phys. Fluids* **12**, 1343–1362.

STAQUET, C. & GODEFERD, F. S. 1998 Statistical modelling and direct numerical simulations of decaying stably stratified turbulence. Part 1. Flow energetics. *J. Fluid Mech.* **360**, 295–340

TAYLOR, G. I. 1935 Statistical theory of turbulence: Parts I-II. *Proc. R. Soc. Lond.* A **151**, 421–64.

WAITE, M. L. & BARTELLO, P. 2004 Stratified turbulence dominated by vortical motion. *J. Fluid Mech.* **517**, 281–308.

WAITE, M. L. & BARTELLO, P. 2006 Stratified turbulence generated by internal gravity waves. *J. Fluid Mech.* **546**, 313–339.